Interfacial Trap#Assisted Triplet Generation in Lead Halide Perovskite Sensitized Solid#State Upconversion

Citation: Wang, L., Yoo, J. J., Lin, T.-A., Perkinson, C. F., Lu, Y., Baldo, M. A., Bawendi, M. G., Interfacial Trap-Assisted Triplet Generation in Lead Halide Perovskite Sensitized Solid-State Upconversion. Adv. Mater. 2021, 33, 2100854

As Published: http://dx.doi.org/10.1002/adma.202100854

Publisher: Wiley

Persistent URL: https://hdl.handle.net/1721.1/140348

Version: Author's final manuscript: final author's manuscript post peer review, without publisher's formatting or copy editing

Interfacial Trap-assisted Triplet Generation in Lead Halide Perovskite Sensitized Solid-state Upconversion

Lili Wang,[a] Jason J. Yoo,[a,c†] Ting-An Lin,[b†] Collin F. Perkinson,[a,b†] Yongli Lu,[a] Marc A. Baldo,[b] Moungi G. Bawendi[a*]*

Dr. L. Wang, Dr. J. J. Yoo, C. F. Perkinson, Y. Lu, Prof. M. G. Bawendi

Department of Chemistry, Massachusetts Institute of Technology, 77 Massachusetts Avenue, Cambridge, Massachusetts 02139, USA

Email: mgb@mit.edu

T.-A. Lin, Prof. M. A. Baldo

Department of Electrical Engineering and Computer Science, Massachusetts Institute of Technology, 77 Massachusetts Avenue, Cambridge, Massachusetts 02139, USA

Email: baldo@mit.edu

Dr. J. J. Yoo

This is the author manuscript accepted for publication and has undergone full peer review but has not been through the copyediting, typesetting, pagination and proofreading process, which may lead to differences between this version and the Version of Record. Please cite this article as doi: 10.1002/adma.202100854.

Current affiliation: Division of Advanced Materials, Korea Research Institute of Chemical Technology, 141 Gajeong-Ro, Yuseong-Gu, Daejeon 34114, Republic of Korea

Keywords: lead halide perovskites, surface treatment, trap-assisted, solid-state near IR-to-visible upconversion

[†] These authors contributed equally to this work.

Photon upconversion via triplet-triplet annihilation (TTA) has promise for overcoming the Shockley–Queisser limit for single-junction solar cells by allowing the utilization of sub-bandgap photons. Recently, bulk perovskites have been employed as sensitizers in solid-state upconversion devices to circumvent poor exciton diffusion in previous nanocrystal-sensitized devices. However, an in-depth understanding of the underlying photophysics of perovskite-sensitized triplet generation is still lacking due to the difficulty of precisely controlling interfacial properties of fully solution-processed devices. In this study, interfacial properties of upconversion devices are adjusted by a mild surface solvent treatment, specifically altering perovskite surface properties without perturbing the bulk perovskite. Thermal evaporation of the annihilator precludes further solvent contamination. Counterintuitively, devices with more interfacial traps show brighter upconversion. Approximately an order of magnitude difference in upconversion brightness is observed across different interfacial solvent treatments. Sequential charge transfer and interfacial trap-assisted triplet sensitization are demonstrated by comparing upconversion performance, transient photoluminescence dynamics, and magnetic field dependence of the devices. Incomplete triplet conversion from transferred charges and consequent triplet-charge annihilation (TCA) are also observed. Our observations highlight the importance of interfacial control and provide guidance for further design and optimization of upconversion devices using perovskites or other semiconductors as sensitizers.

Photon upconversion describes a process that converts two or more low-energy photons into a single high-energy photon. By allowing the collection of sub-bandgap photons, upconversion shows promise for overcoming the Shockley–Queisser limit for single-junction solar cells and for

replacing costly infrared photodetectors with inexpensive upconversion-sensitized silicon photodetectors.[1–4] Compared to other upconversion processes including multiphoton absorption in lanthanide nanoparticles and sum-frequency generation in nonlinear crystals, triplet-triplet annihilation based upconversion (TTA-UC) is particularly suitable for solar applications due to the advantage of efficient conversion at low photon fluxes.[5–8] In a TTA-UC device, a sensitizer is employed as the absorber and the spin-mixer to convert the optically excited singlet exciton to the triplet state of the annihilator. Recombination of two triplet states on adjacent annihilator molecules then generates a higher-lying emissive singlet state to achieve upconversion.

Previous nanocrystal (NC)-sensitized solid-state TTA-UC devices suffer from poor exciton diffusion in the sensitizer layer, which limits the sensitizer thickness to only one to two monolayers.[9,10] The resulting low device absorption and high upconversion threshold preclude their potential utility for solar applications. The recent discovery of bulk perovskites as an alternative triplet sensitizer in solid-state near-infrared to visible upconversion devices provides a new path to circumvent the issue of poor exciton diffusion.[11,12] The combination of high absorption cross section,[13] long carrier lifetimes,[14,15] and bandgap tunability of bulk perovskites[16] render them more suitable candidates for solid-state upconversion compared to nanocrystals. Despite the growing research interest in perovskite-sensitized upconversion devices, the underlying photophysics of perovskite-sensitized triplet generation and subsequent TTA-upconversion still remain highly underexplored. Unlike quantum-confined excitons in NCs, photogenerated excitons in a bulk perovskite will rapidly dissociate into free electrons and holes within picoseconds.[17] An in-depth understanding of charge injection into the triplet state of the annihilator at the perovskite-annihilator interface is of utmost importance for guiding perovskite-sensitized upconversion device

optimization and future device design with other bulk semiconductors.

To date, all reported bulk perovskite-sensitized TTA-UC devices are fully solution-processed by either spin-coating the organic annihilator layer onto the perovskites or directly incorporating the annihilator into the anti-solvent,[11,12,18–21] which poses an obstacle to unravelling the detailed photophysics of perovskite-sensitized upconversion. Perovskites are notoriously sensitive to solvent exposure and fabrication conditions. The additional spin-coating process can perturb both the perovskite properties and the packing morphology of the annihilator molecules, consequently affecting charge injection and triplet sensitization at the interface.[20,22] Directly incorporating the annihilator into the anti-solvent may also impact perovskite crystallization and formation during the annealing step. Varying the fabrication conditions of perovskites to test their effects on upconversion is complicated because this simultaneously varies multiple parameters in perovskites, thus making it difficult to disentangle the contributing factors in the photophysics. For example, changing the thickness of bulk perovskites is typically accompanied by changes in grain size, surface morphology, and phase purity.[23,24]

In this work, we investigate the effects of interfacial properties on perovskite-sensitized upconversion and provide evidence of interfacial trap-assisted triplet sensitization. To overcome the above-mentioned difficulties, we replace spin-coating with thermal evaporation to fabricate the annihilator layer and adopt a surface treatment strategy that selectively alters the interfacial properties of perovskites without perturbing the bulk. This mild solvent treatment modifies surface trap densities of the perovskites. Counterintuitively, steady-state photoluminescence measurements reveal a positive correlation between interfacial trap densities and upconversion efficiencies in perovskite-sensitized upconversion devices. Brighter upconversion observed in devices with more

interfacial traps suggests interfacial trap-assisted triplet generation. These observations highlight the importance of controlling interfacial properties in device optimization and inform future design of solid-state perovskite-sensitized upconversion devices.

The solid-state upconversion devices in this study are fabricated as bilayer devices consisting of a $MA_{0.15}FA_{0.85}PbI_3$ film and a subsequent layer of rubrene doped with 1% dibenzotetraphenylperiflanthene (DBP), as shown in Figure 1a. The absorption (solid lines) and emission (dashed lines) spectra of the perovskite and the upconversion device are shown in Figure 1b with a picture of the upconversion device in the inset. The band diagrams of $MA_{0.15}FA_{0.85}PbI_3$ perovskite and rubrene are shown in Figure 1c. This band alignment favors hole transport from the valence band maximum (VBM) of the perovskite to the highest occupied molecular orbital (HOMO) of rubrene.[25,26] Direct electron transport from the conduction band minimum (CBM) of the perovskite to the lowest unoccupied molecular orbital (LUMO) of rubrene is energetically disallowed due to a ~1 eV energy offset.[25] Previous reports on perovskite/rubrene upconversion devices have confirmed triplet sensitization at the perovskite/rubrene interface and suggest sequential charge transfer as a possible mechanism for triplet sensitization.[11,12,20,21] However, understanding of charge injection and triplet sensitization at the interface of perovskite-sensitized upconversion devices is still limited due to the difficulty of selectively controlling interfacial properties.

To gain better control at the perovskite interface and investigate its effects on triplet sensitization and upconversion, we adopt a mild surface treatment strategy that selectively modifies the interfacial properties of perovskites without affecting properties of the bulk. The perovskites are fabricated and treated with either isopropyl alcohol (IPA) or toluene for 30 s in a nitrogen-filled

glovebox with O_2 and H_2O concentrations below 0.1 ppm. For device fabrication, rubrene with 1% DBP is then thermally evaporated onto the perovskites to preclude further solvent influences.

The PL spectra (Figure 2a) and lifetimes (Figure 2b) of perovskites with and without solvent treatments are identical, indicating that the applied solvent treatments are mild enough to maintain perovskite bulk properties. To further examine the solvent treatment effects, we characterize the perovskites with surface-sensitive techniques, including scanning electron microscopy (SEM), grazing incidence X-ray diffraction (GIXRD), and X-ray photoelectron spectroscopy (XPS). No obvious differences are observed between the SEM images of as-prepared and toluene-treated perovskites (Figure 2c and 2e). In contrast, IPA treatment creates visible pinholes on the surface of perovskite, as pointed with red arrows in Figure 2d. The XRD pattern of IPA-treated perovskites reveals an additional set of low-intensity peaks (marked with # and yellow lines in Figures 2f and 2g) that are consistent with reported peaks of PbI_2, confirming the formation of trace PbI_2.[27,28] The presence of metallic Pb^0 on the surface of perovskites is also demonstrated by XPS, with a lower Pb^0 content in the toluene-treated perovskites than in the IPA-treated perovskites, as shown in Figure 2h. The surface characterization differences among these perovskites can be explained by the solubility of perovskites in the applied solvents. IPA can effectively dissolve formamidinium iodide (FAI) and methylammonium iodide (MAI) due to its high polarity and ability to form hydrogen bonding, whereas toluene is frequently used as an anti-solvent for perovskites and shows very low solubility towards these organic halide precursors. To test the solubility of perovskites, we place perovskites in IPA-d_8 or toluene-d_8 overnight and measure ^{1}H NMR spectra of the resulting solutions. As shown in Figure 2i, the ^{1}H NMR spectrum of the perovskite in IPA-d_8 reveals dissolution of organic halides from the perovskite. Because of hydrogen bonding between IPA-d_8 and organic halides in perovskite,

small chemical shifts in the NMR peaks are observed when compared to the spectra of saturated MAI and FAI solutions. In contrast, no detectable NMR signals of MAI or FAI are observed from perovskite in toluene-d_8 (Figure S1). Hence, the IPA-treatment for 30 s mildly removes trace organic halides from the perovskite, creating iodide vacancies, residual PbI_2, and visible pinholes on the surface, as proven by SEM and XRD measurements. In contrast to IPA, which creates more iodide vacancies on the perovskite, toluene can remove trace residual solvent from the perovskite that is left after the initial annealing of the perovskite fabrication process and reduce surface traps. The iodide vacancies are able to trap photogenerated electrons and induce disproportionation of Pb^{2+} to generate metallic Pb^0.[29,30] Therefore, the Pb^0 content measured by XPS indicates the relative surface trap densities in the as-prepared and solvent-treated perovskites.

To characterize the effect of this surface treatment on upconversion, we thermally evaporate rubrene:1%DBP onto the as-prepared and solvent-treated perovskites and compare the upconversion performance of these devices. We first compare their upconversion efficiencies using the integrating sphere measurement techniques proposed by de Mello et al.[31] The external quantum efficiency (EQE) of an upconversion device is the ratio of the number of upconverted photons to the number of low-energy incident photons and can be written as

$$EQE = Abs \cdot \varphi_{ET} \frac{\varphi_{TTA}}{2} \cdot \varphi_{PL} \qquad (1)$$

where *Abs* is the absorption of the device at 785 nm excitation, φ_{ET} is the efficiency of triplet transfer from the perovskite to the rubrene:1%DBP layer, φ_{TTA} is the TTA efficiency, and φ_{PL} is the PLQY of rubrene:1%DBP, which is measured to be 45.6% at 450 nm. The upconversion efficiency

φ_{UC} is defined as the fraction of absorbed photons that result in singlet excitons in the annihilator, represented as

$$\varphi_{UC} = \frac{EQE}{Abs \cdot \varphi_{PL}} \cdot 2 \qquad (2)$$

from equation (1), with the factor of two scaling the maximum of φ_{UC} to 100%.[5] The upconversion efficiencies of our devices are summarized in Table 1. Interestingly, the upconversion efficiencies exhibit excitation power dependency even at moderate excitation powers due to the bulk semiconductor nature of the perovskites. The upconverted PL brightness of three devices at selected excitation power are shown in Figure 3a. Although the relative ratio of upconverted PL varies with excitation power, the IPA treatment improves upconversion brightness compared to the control device, while the toluene treatment reduces the upconversion brightness.

In addition to upconversion efficiency, the threshold intensity is another important factor for potential practical applications of TTA-UC. The upconverted PL in a TTA-based upconversion device has a unique dependence on the excitation intensity due to the competition between bimolecular TTA and first-order nonradiative triplet loss. The transition point represents the threshold intensity at which TTA is efficient enough to dominate over triplet loss in the upconversion devices. The excitation intensity dependence of upconverted PL in our devices is depicted in Figure 3b, with the threshold intensities determined to be 61.0 mW/cm^2, 123.8 mW/cm^2, and 303.5 mW/cm^2 for the upconversion devices made from IPA-treated, as-prepared, and toluene-treated perovskites, respectively, indicating that TTA is most efficient in the IPA-treated upconversion device. A detailed discussion on the fitting method used to determine threshold intensities is included in the Supporting Information. The trend in upconversion efficiencies and threshold intensities among

these three devices suggests a positive correlation between upconversion performance and surface trap densities of perovskites, favoring a trap-assisted triplet sensitization mechanism.

The effect of IPA treatment time on the upconversion brightness is also examined. As the treatment time increases from 30 s to 180 s, pinhole passivation and formation of more flakes on the perovskites are observed from SEM images (Figure S2), consistent with continuous PbI_2 formation that is shown by XRD patterns (Figure S3). However, the upconversion brightness of IPA-treated devices (Figure S4, with the integrated brightness trend shown in the inset) exhibits a slightly different trend. The brightness reaches a maximum at a treatment time of 30 s and declines with further treatment, but it still remains superior to the device made from as-prepared perovskite. This trend further excludes PbI_2 formation as a possible explanation for the upconversion enhancement observed in the IPA-treated devices.

To understand the underlying physical reasons for the differences in upconversion performance, we measure the transient PL dynamics of the upconversion devices and the magnetic field effect of their upconverted PL. As the incident power increases, the PL dynamics of the perovskite-only film (Figure 4a) exhibit a reduced early-time quenching due to trap filling and a dominant long component that is accelerated due to the bimolecular nature of free carrier recombination. In upconversion devices, the bulk carrier recombination of perovskites is quenched due to hole transfer to the rubrene layer, as shown in Figure 4b. All three devices show significant quenching of the long-lifetime component at low fluences compared to the perovskite-only film. The quenching observed in the IPA-treated device is similar to that observed in the control devices while the quenching observed in the toluene-treated device is slightly less.

The perovskite PL dynamics in upconversion devices is also power-dependent, consistent with previous literatures on similar perovskite/Rub:DBP systems.[12,20,21,32] All three devices (Figure 4c–e) present similar trends with less efficient PL quenching at higher incident power. This power dependence difference is likely due to both competition with bulk carrier recombination and charge accumulation at the perovskite/rubrene interface that can lead to triplet-charge annihilation (TCA). As the power increases, a larger triplet population is generated, increasing TCA and back-transfer from the Rub/DBP singlet to perovskite and resulting in less quenching of the long-lifetime component observed by transient PL measurements. TCA is an energy loss pathway in upconversion devices that results in triplet exciton dissociation back to charges and nonradiative triplet exciton loss, negatively affecting the upconversion performance. The presence of TCA can be identified from the magnetic field effect (MFE) of the upconverted PL by its positive dependence on magnetic field, which is distinct from the negative curve of TTA according to the model proposed by Merrifield et al.[33–35] The MFE magnitudes of the three upconversion devices are shown in Figure 4f and confirms the interplay between TTA and TCA. The MFE magnitude of the device is presented as the percentage change of upconverted PL under magnetic field. Although the magnitudes of MFE suggest an escalating competition between TCA and TTA in the IPA-treated device compared to the other two devices, the effect of TCA is not strong enough to overturn the upconversion brightness trend among the three devices. These observations further suggest that there is a higher triplet population in the IPA-treated device due to efficient triplet generation, which is consistent with the transient dynamics of the upconverted PL of the devices shown in Figure S5.

The combination of power-dependent transient PL dynamics and MFE measurements strongly confirms sequential charge transfer as the dominant mechanism for triplet sensitization, in

which a hole transfers first from perovskite to rubrene and subsequently recombines with the residing electron at the interface to form a bound triplet exciton. The efficiency of this interfacial recombination is non-unity, however, leading to charge accumulation and TCA in the upconversion devices. The significantly enhanced upconversion brightness of the IPA-treated device cannot be completely explained by its trivial charge extraction difference compared to the control device. Instead, our results suggest that more triplets form in the IPA-treated device due to efficient interfacial recombination that is trap-assisted. Trap state- mediated triplet transfer has been previously demonstrated in several excitonic systems with NC sensitizers. [36–38] For example, $CuInS_2$ NCs, in which the photogenerated excitons are self-trapped due to hole localization to intragap Cu states, can efficiently transfer triplets to surface- anchored anthracene.[38] Formation of surface intermediate states is also reported in the triplet transfer from PbS NC to TIPS-pentacene molecules. [37] For charge-initiated triplet sensitization, one prerequisite for interfacial recombination is that the residing electron in the perovskite and the transferred hole in rubrene must be in close proximity due to the rather localized wavefunction of the triplet exciton. For materials with high carrier mobilities, such as perovskites, the carriers can rapidly diffuse away from the critical distance of triplet formation before they recombine. Shallow interfacial traps are able to slow carrier diffusion and localize carriers, thereby increasing the probability of interfacial recombination. Intuitively, interfacial traps act as a bridge for triplet sensitization, with higher trap density representing a wider bridge that allows for more triplet formation.

In conclusion, we demonstrate sequential charge transfer and trap-assisted triplet sensitization at the interface of perovskite-sensitized TTA devices by mildly adjusting their interfacial properties of upconversion and analyzing their differences in upconversion performance, transient

PL dynamics, and magnetic field effect. Non-unity conversion of the transferred holes into triplets and consequent TCA between the triplets and residual charges are observed to negatively impact upconversion performance. Our observations can serve as a guide for the future design and optimization of solid-state upconversion devices using perovskites or other bulk semiconductors as sensitizer. Charge-initiated triplet sensitization in these devices is particularly sensitive to their interfacial structures. Therefore, fine-tuning the interfacial structure of these sensitizers without damaging their superior bulk properties is an inevitable step toward improving the upconversion efficiency of these devices. Further optimization of perovskite-sensitized upconversion in a bilayer device structure would require perovskites with long carrier lifetimes that allow carriers to effectively diffuse towards the interface before they recombine, and with a high density of surface traps that serve as interfacial recombination centers for improving the triplet formation efficiency toward unity.

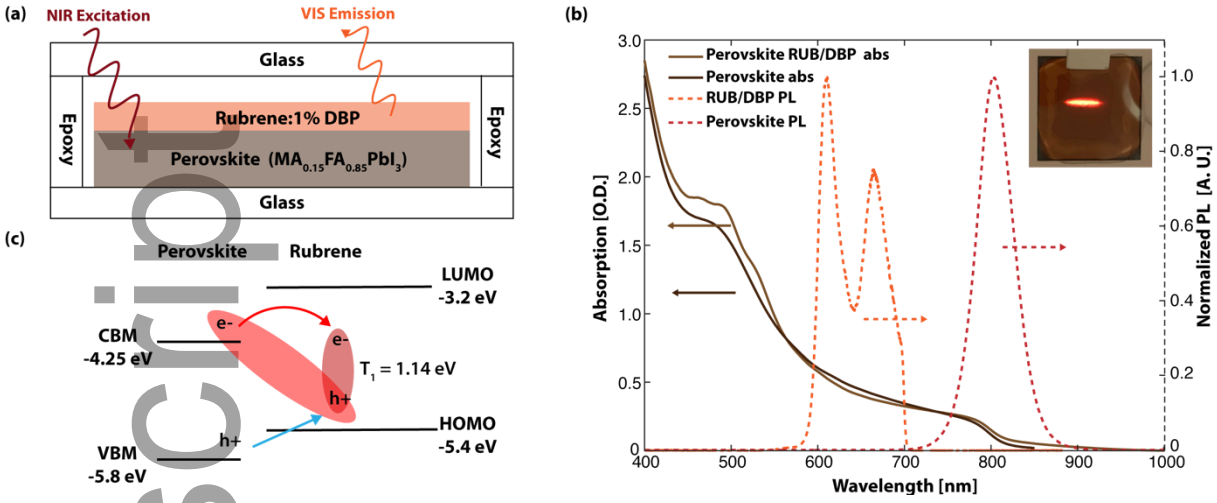

Figure 1. a) Schematic representation of the perovskite-sensitized solid-state NIR-to-visible upconversion device. b) Absorption (solid lines) and normalized emission (dashed lines) spectra of $MA_{0.15}FA_{0.85}PbI_3$ perovskite film and the bilayer upconversion device. A 700 nm shortpass filter was applied in collecting the upconverted PL to minimize laser scattering and residual perovskite signal at higher wavelengths. The inset is a photo of the device under 785 nm excitation. c) Band diagrams of $MA_{0.15}FA_{0.85}PbI_3$ and rubrene doped with 1 wt.% DBP favoring hole transport from the VBM of the perovskite to the HOMO of rubrene. Electron transfer from the CBM of the perovskite to the LUMO of rubrene is energetically disallowed due to a ~ 1eV barrier, but a bound triplet exciton can be formed in rubrene.

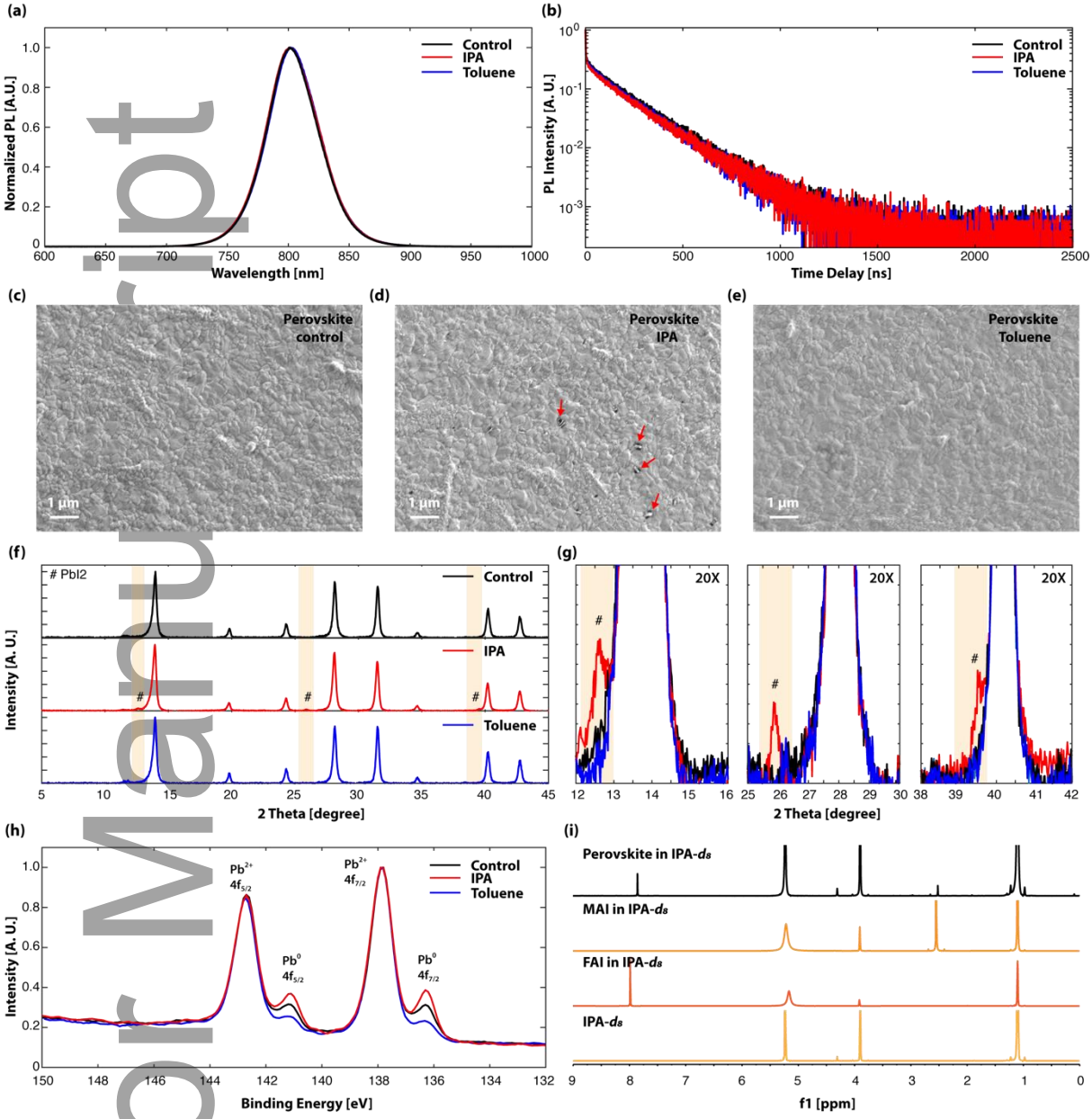

Figure 2. a) As-prepared, IPA-treated, and toluene-treated $MA_{0.15}FA_{0.85}PbI_3$ perovskite films exhibit identical emission spectra. b) Transient PL dynamics of $MA_{0.15}FA_{0.85}PbI_3$ perovskite films remain unperturbed with IPA or toluene treatment. c–e) SEM images of the as-prepared, IPA-treated, and toluene-treated perovskite films, respectively. IPA treatment creates pinholes on the perovskite surface, as pointed with red arrows shown in panel d. f) GIXRD patterns of the perovskite films with different solvent treatments. # denotes the PbI_2 diffraction peaks. g) 20× magnification on the vertical axis of XRD patterns reveals PbI_2 formation in the IPA-treated perovskite. h) XPS spectra of

perovskites reveal different content of metallic Pb^0 formation on the perovskite surface: IPA-treated > as-prepared > toluene-treated perovskites. i) NMR spectra of perovskite, MAI, FAI, and neat IPA-d_8 solvent (from top to bottom) demonstrate dissolution of MAI and FAI precursors during IPA treatment.

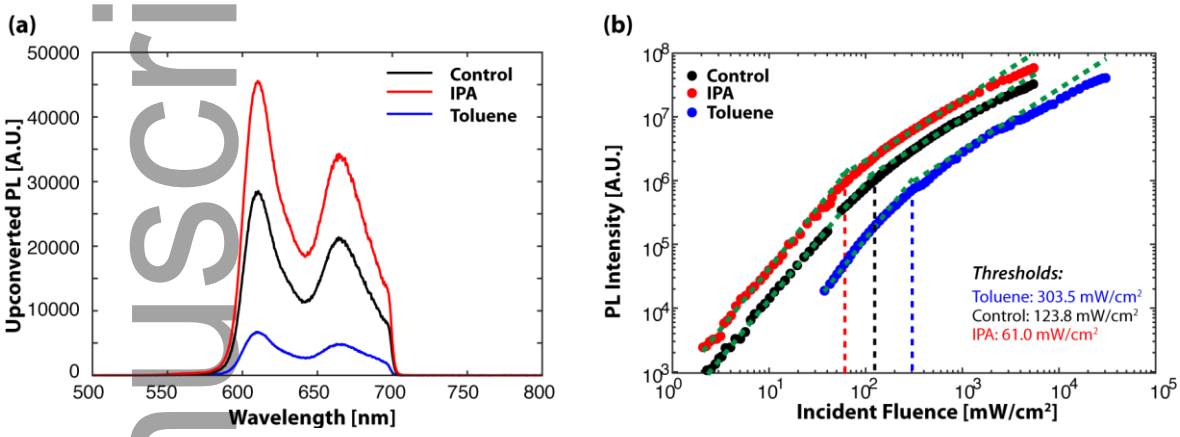

Figure 3. a) The upconverted photoluminescence of the upconversion devices made with different solvent-treated perovskites, excited at 785 nm. b) Excitation fluence dependence of the upconverted PL of the bilayer devices, showing that the device made with IPA-treated perovskite is the most efficient and exhibits the lowest upconversion threshold among all three devices. The upconversion thresholds are denoted by dashed lines. The fitted slopes for the devices are: Control: 1.8 to 0.9; IPA: 1.8 to 0.9; Toluene: 1.9 to 0.9.

Table 1. Summary of the device performance at different excitation powers. EQE: external quantum efficiency. φ_{UC}: upconversion efficiency. The performance of toluene-treated device at low powers are not included because the upconversion brightness is too dim to be reliably measured with integrating sphere.

	Control Device			IPA-treated Device			Toluene-treated Device		
Power [mW/cm^2]	Abs [%]	EQE [%]	φ_{UC} [%]	Abs [%]	EQE [%]	φ_{UC} [%]	Abs [%]	EQE [%]	φ_{UC} [%]

2746	30.07	0.009	0.131	31.17	0.014	0.197	30.48	0.003	0.043
953	31.00	0.013	0.184	31.50	0.021	0.293	30.29	0.005	0.072
241	32.30	0.023	0.313	32.87	0.032	0.427	31.52	0.006	0.084
184	29.84	0.022	0.324	31.44	0.032	0.447	-	-	-
93.3	30.34	0.018	0.255	33.23	0.037	0.489	-	-	-

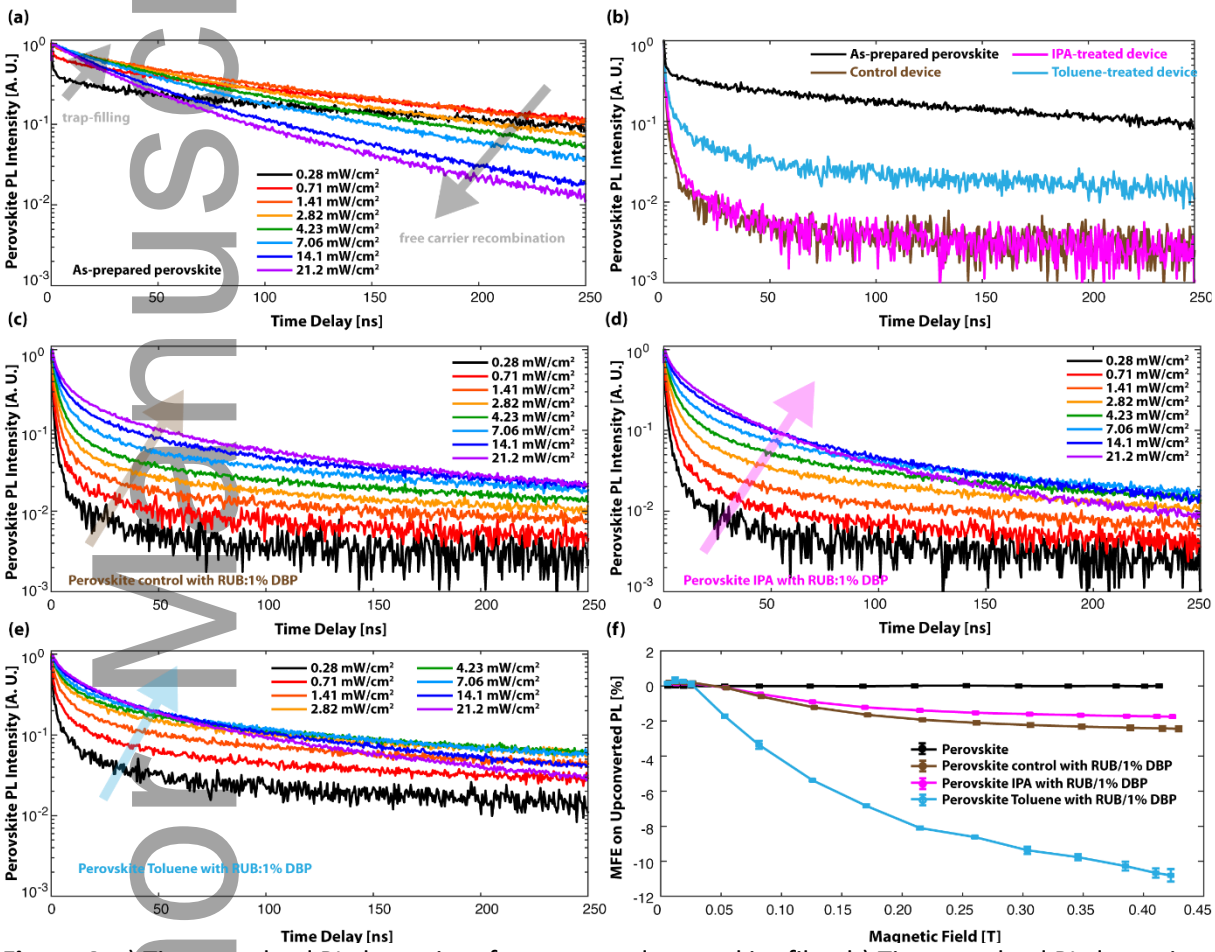

Figure 4. a) Time-resolved PL dynamics of as-prepared perovskite film. b) Time-resolved PL dynamics of the perovskite emission from the $MA_{0.15}FA_{0.85}PbI_3$ film (black) and the bilayer devices with different solvent-treated perovskites (colored) at 40 nW. c–e) Excitation fluence dependence of the quenched perovskite emission from the bilayer upconversion device with as-prepared, IPA-treated, and toluene-treated perovskites, respectively. f) Change of the upconverted PL of the perovskite and the devices with different solvent-treated perovskites under an applied magnetic field. The MFE

magnitude differences of the three devices reveal competition between two processes: triplet-triplet annihilation and triplet-charge annihilation.

Experimental Section

Sample Preparation: The details of the sample preparation are described in the Supporting Information.

Characterizations: The details of all the measurements and the necessary theories are described in the Supporting Information.

Supporting Information

Supporting Information is available from the Wiley Online Library or from the authors.

Acknowledgements

L.W. (device design, characterization, and analysis) was funded by the U.S. Department of Energy, Office of Basic Energy Sciences, Division of Materials Sciences and Engineering, under award no. DE-FG02-07ER46454. J. J. Y. (assisted with perovskite fabrication) was funded by the U.S. Army Research Office through the Institute for Soldier Nanotechnologies, under contract no. W911NF-13-D-0001 and by the National Aeronautics and Space Administration (NASA) under grant no. NNX16AM70H. T. L. (assisted with thermal evaporation, PL, and quantum yield measurements) and C.F.P. (assisted with thermal evaporation, PL, and magnetic field measurements) were funded by the U.S. Department of Energy, Office of Basic Energy Sciences under award no. DE-FG02-07ER46474. C.F.P. also acknowledges a National Science Foundation Graduate Research Fellowship under grant no. 1122374.

J.J.Y., T.L., and C.F.P. contributed equally to this work.

Received: ((will be filled in by the editorial staff))
Revised: ((will be filled in by the editorial staff))
Published online: ((will be filled in by the editorial staff))

References:

[1] F.-L. Meng, J.-J. Wu, E.-F. Zhao, Y.-Z. Zheng, M.-L. Huang, L.-M. Dai, X. Tao, J.-F. Chen, *Nanoscale* **2017**, *9*, 18535.

[2] M. He, X. Pang, X. Liu, B. Jiang, Y. He, H. Snaith, Z. Lin, *Angew. Chemie Int. Ed.* **2016**, *55*, 4280.

[3] T. Trupke, M. A. Green, P. Würfel, *J. Appl. Phys.* **2002**, *92*, 1668.

[4] W. Shockley, H. J. Queisser, *J. Appl. Phys.* **1961**, *32*, 510.

[5] J. Zhou, Q. Liu, W. Feng, Y. Sun, F. Li, *Chem. Rev.* **2015**, *115*, 395.

[6] T. N. Singh-Rachford, F. N. Castellano, *Coord. Chem. Rev.* **2010**, *254*, 2560.

[7] M. Mahboub, Z. Huang, M. L. Tang, *Nano Lett.* **2016**, *16*, 7169.

[8] G. Tessitore, G. A. Mandl, M. G. Brik, W. Park, J. A. Capobianco, *Nanoscale* **2019**, *11*, 12015.

[9] M. Wu, D. N. Congreve, M. W. B. Wilson, J. Jean, N. Geva, M. Welborn, T. Van Voorhis, V. Bulović, M. G. Bawendi, M. A. Baldo, *Nat. Photonics* **2015**, *10*, 31.

[10] L. Nienhaus, M. Wu, V. Bulović, M. A. Baldo, M. G. Bawendi, *Dalt. Trans.* **2018**, *47*, 8509.

[11] L. Nienhaus, J.-P. Correa-Baena, S. Wieghold, M. Einzinger, T.-A. Lin, K. E. Shulenberger, N. D. Klein, M. Wu, V. Bulović, T. Buonassisi, M. A. Baldo, M. G. Bawendi, *ACS Energy Lett.* **2019**, *4*, 888.

[12] S. Wieghold, A. S. Bieber, Z. A. VanOrman, L. Daley, M. Leger, J.-P. Correa-Baena, L. Nienhaus, *Matter* **2019**, *1*, 705.

[13] S. De Wolf, J. Holovsky, S.-J. Moon, P. Löper, B. Niesen, M. Ledinsky, F.-J. Haug, J.-H. Yum, C. Ballif, *J. Phys. Chem. Lett.* **2014**, *5*, 1035.

[14] G. Xing, N. Mathews, S. Sun, S. S. Lim, Y. M. Lam, M. Grätzel, S. Mhaisalkar, T. C. Sum, *Science (80-.).* **2013**, *342*, 344.

[15] S. D. Stranks, G. E. Eperon, G. Grancini, C. Menelaou, M. J. P. Alcocer, T. Leijtens, L. M. Herz, A. Petrozza, H. J. Snaith, *Science (80-.).* **2013**, *342*, 341.

[16] S. Tao, I. Schmidt, G. Brocks, J. Jiang, I. Tranca, K. Meerholz, S. Olthof, *Nat. Commun.* **2019**,

10, 2560.

[17] C. S. Ponseca, T. J. Savenije, M. Abdellah, K. Zheng, A. Yartsev, T. Pascher, T. Harlang, P. Chabera, T. Pullerits, A. Stepanov, J.-P. Wolf, V. Sundström, *J. Am. Chem. Soc.* **2014**, *136*, 5189.

[18] K. Prashanthan, B. Naydenov, K. Lips, E. Unger, R. W. MacQueen, *J. Chem. Phys.* **2020**, *153*, 164711.

[19] S. Wieghold, A. S. Bieber, J. Lackner, K. Nienhaus, G. U. Nienhaus, L. Nienhaus, *ChemPhotoChem* **2020**, *4*, 704.

[20] S. Wieghold, L. Nienhaus, *J. Phys. Chem. Lett.* **2020**, *11*, 601.

[21] S. Wieghold, A. S. Bieber, Z. A. VanOrman, L. Nienhaus, *J. Phys. Chem. Lett.* **2019**, *10*, 3806.

[22] J. J. Yoo, S. Wieghold, M. C. Sponseller, M. R. Chua, S. N. Bertram, N. T. P. Hartono, J. S. Tresback, E. C. Hansen, J.-P. Correa-Baena, V. Bulović, T. Buonassisi, S. S. Shin, M. G. Bawendi, *Energy Environ. Sci.* **2019**, *12*, 2192.

[23] A.-N. Cho, I.-H. Jang, J.-Y. Seo, N.-G. Park, *J. Mater. Chem. A* **2018**, *6*, 18206.

[24] T. Du, W. Xu, S. Xu, S. R. Ratnasingham, C.-T. Lin, J. Kim, J. Briscoe, M. A. McLachlan, J. R. Durrant, *J. Mater. Chem. C* **2020**, *8*, 12648.

[25] G. Ji, G. Zheng, B. Zhao, F. Song, X. Zhang, K. Shen, Y. Yang, Y. Xiong, X. Gao, L. Cao, D.-C. Qi, *Phys. Chem. Chem. Phys.* **2017**, *19*, 6546.

[26] P. Qin, J. Zhang, G. Yang, X. Yu, G. Li, *J. Mater. Chem. A* **2019**, *7*, 1824.

[27] A. Bahtiar, S. Rahmanita, Y. D. Inayatie, *IOP Conf. Ser. Mater. Sci. Eng.* **2017**, *196*, 12037.

[28] J. F. Condeles, R. A. Ando, M. Mulato, in *J. Mater. Sci.*, Springer, **2008**, pp. 525–529.

[29] C. Das, M. Wussler, T. Hellmann, T. Mayer, W. Jaegermann, *Phys. Chem. Chem. Phys.* **2018**, *20*, 17180.

[30] X. Tang, M. Brandl, B. May, I. Levchuk, Y. Hou, M. Richter, H. Chen, S. Chen, S. Kahmann, A. Osvet, F. Maier, H.-P. Steinrück, R. Hock, G. J. Matt, C. J. Brabec, *J. Mater. Chem. A* **2016**, *4*, 15896.

[31] J. C. de Mello, H. F. Wittmann, R. H. Friend, *Adv. Mater.* **2004**, *9*, 230.

[32] S. Wieghold, A. S. Bieber, Z. A. VanOrman, A. Rodriguez, L. Nienhaus, *J. Phys. Chem. C* **2020**,

124, 18132.

[33] R. E. Merrifield, *J. Chem. Phys.* **1968**, *48*, 4318.

[34] R. E. Merrifield, P. Avakian, R. P. Groff, *Chem. Phys. Lett.* **1969**, *3*, 155.

[35] V. Ern, R. E. Merrifield, *Phys. Rev. Lett.* **1968**, *21*, 609.

[36] T. Jin, T. Lian, *J. Chem. Phys.* **2020**, *153*, 74703.

[37] J. A. Bender, E. K. Raulerson, X. Li, T. Goldzak, P. Xia, T. Van Voorhis, M. L. Tang, S. T. Roberts, *J. Am. Chem. Soc.* **2018**, *140*, 7543.

[38] Y. Han, S. He, X. Luo, Y. Li, Z. Chen, W. Kang, X. Wang, K. Wu, *J. Am. Chem. Soc.* **2019**, *141*, 13033.

TOC entry:

The effect of interfacial properties on charge-initiated triplet sensitization in perovskite-sensitized solid-state upconversion devices is investigated. Trap-assisted triplet sensitization is demonstrated via modifying interfacial trap densities of the devices through surface treatment while monitoring the upconversion performance. Devices with more interfacial traps show brighter upconversion, highlighting the importance of interfacial control in perovskite sensitized upconversion devices.

ToC figure: